Progress In Electromagnetics Research C, Vol. 137, 235–249, 2023

Hybrid-Vector Model Predictive Flux Control for PMSM Considering Narrow Pulse

Qianghui Xiao[1], Zhi Yu[1], Wenting Zhang[1], Zhongjian Tang[1], and Zhun Cheng[2, *]

Abstract—Multi-vector model predictive control (MPC) of permanent magnet synchronous motors (PMSM) has two issues: selecting the optimal voltage vector (VV) combination is very complicated, and multiple prediction calculations to minimize the cost function result in a heavy computational burden; applying a VV with a short duration may generate narrow pulses, while the effect of reducing torque ripples and stator current harmonics is not obvious. The hybrid-vector model prediction flux control (HV-MPFC) strategy considering narrow pulse suppression is proposed in this paper. First, the optimal VV combination is quickly identified by the sector where the stator flux error vector is located, which lowers the control complexity and computational burden. Secondly, by the relationship between the action time of three VVs and the set time threshold, the hybrid-vector strategy to switch among three VVs, two VVs, and a single VV is employed to prevent the generation of narrow pulses. Finally, experimental results show that, compared with the existing three-vector MPC strategy, the HV-MPFC strategy effectively suppresses the generation of narrow pulses and achieves smaller torque ripples and stator current harmonics at the same switching frequency.

1. INTRODUCTION

PMSM has the advantages of high efficiency, high power density, and high reliability and has been widely used in industrial fields [1–3]. To meet the different control requirements of different applications on the performance of the transmission system, control strategies with different advantages have been proposed. In the past, the most representative ones were the field-oriented control (FOC) and direct torque control (DTC) [4, 5]. FOC is used on many occasions due to its good steady-state performance, but its dynamic performance needs to be improved. The difference is that DTC relies on a direct hysteresis comparator and switch table, which has a fast dynamic response, but has disadvantages such as large steady-state torque ripples and unfixed switching frequency [6, 7].

For achieving simpler and more effective control, model predictive control (MPC) has gradually become a hot research topic in recent years [8]. Due to the inherent discrete characteristics of the two-level voltage source inverter, the MPC strategy can be used to predict the future state of the motor under the action of each VV, and the optimal VV for the next control period can be selected through the evaluation of the designed cost function. Compared with the FOC strategy, MPC eliminates the current regulator in FOC, and the dynamic response is faster [9]. Compared with the DTC strategy, MPC has a similar dynamic response, and the selected VV is more accurate [10]. Based on the control objective, FCS-MPC is divided into two major types: model predictive current control (MPCC) and model predictive torque control (MPTC). MPCC aims to control d-axis and q-axis currents, while MPTC controls torque and stator flux. The cost function of MPTC based on torque and flux errors requires the design of suitable weighting factors, which is necessary because of the different units between torque

Received 2 July 2023, Accepted 2 September 2023, Scheduled 14 September 2023
* Corresponding author: Zhun Cheng (120277982@qq.com).
[1] Hunan University of Technology, Zhuzhou 412007, China. [2] Hunan Railway Professional Technology College, Zhuzhou 412001, China.

and flux. However, the tuning of the weighting factors is an uphill task due to the lack of theoretical design methods [11]. Model predictive flux control (MPFC) avoids the design of weighting factors by converting the control of torque and flux magnitude into the control of the stator flux vector. The simplified stator flux vector control objective is used as a criterion for selecting the optimal VV [12].

For finite control set MPC, a single VV for one control period limits torque and flux control accuracy. An effective way to improve control accuracy is to increase the number of VVs. Thus, MPC can be classified as single-vector [13] and multi-vector [14–19] MPC according to the number of VVs in one control period. The single-vector MPC strategy is simple and has good dynamic performance, but the steady-state control performance needs to be improved [15]. To improve the steady-state control performance of the system, the double-vector MPC that applies two VVs in one control period to synthesize the target VV is proposed in [11]. Virtual VVs are introduced in [12, 20, 21], which expand the number of VVs to 38 and improve the system control performance. However, these MPC methods for synthesizing finite VVs still cannot satisfy the higher control accuracy requirements. To further improve the control performance, the three-vector MPC with three VVs applied in one control period is proposed in [22, 23], which includes two non-zero VVs and one zero VV. However, since three VVs are included in one control period, the search for the optimal VV combination is complicated, and the calculation burden is heavy. [24] proposes two novel multi-vector MPCC methods for reducing torque and flux ripples, as well as the computational burden. However, there are VVs with shorter duration. Applying a VV with a short duration may generate narrow pulses, while the effect of reducing torque ripples and stator current harmonics is not obvious.

To address the problem of the high computational burden of multi-vector MPC, many improved algorithms have been proposed to reduce the number of candidate VVs and the times of prediction. A new VV optimization strategy was adopted in [20] to reduce the number of candidate VVs from 38 to 13, which significantly reduces the computational effort without affecting the control performance. An optimal VV selection method similar to the direct torque control strategy was proposed in [25], which reduced the virtual candidate VVs from 38 to 12 by using information about the sector where the stator flux vector was located and the torque and flux errors. A method combining direct torque control and the novel deadbeat principle was proposed in [21] to reduce the virtual VV range to one sector. According to the sector where the reference voltage is placed, [11, 26, 27] optimize the VV selection process using the deadbeat principle to narrow the range of candidate VVs. These approaches lighten the computing load, but they do not account for the possibility of narrow pulses being produced by the anticipated VV action time.

In a PWM inverter-fed PMSM drive, an appropriate dead time (T_{dead}) must be inserted in the drive signal to prevent shoot-through in the DC link caused by the simultaneous conduction of both switches in one inverter leg [28]. Traditionally, to reduce switching losses, the minimum pulse width (T_{mpw}) is usually limited. Pulses less than the minimum width will not pass to the gate drive circuit, resulting in failure to turn on the switch. Since the drive signals of the upper and lower switches in the same leg are complementary, pulses larger than the maximum width will result in failure to turn off the switch. The pulse based dead-time compensator (PBDTC) method is an efficient way to compensate for dead-time effects [29]. The minimum pulse width and the compensation of dead time will limit the effective range of the VV in MPFC, affecting the control effect of torque and flux.

In this paper, a hybrid-vector MPFC strategy considering narrow pulse suppression is proposed. The approach utilizes a hybrid VV strategy, switching among three VVs, two VVs, and a single VV to prevent the generation of narrow pulses, and quickly selecting the best VV combination based on the sector where the stator flux error vector is located. Compared with the existing three-VV-operated MPC (3VMPC) schemes as presented in [24], HV-MPFC achieves smaller torque ripples and stator current harmonics at the same switching frequency. Moreover, HV-MPFC can flexibly adjust the contradiction between stator current harmonics and torque ripples and switching frequency by changing the set time threshold, so that the system switching frequency can be reduced without significantly reducing the stator current harmonics and torque ripples. The experimental results verified the validity of the proposed method.

2. PMSM MODEL AND FLUX PREDICTION MODEL

2.1. PMSM Model

In this paper, a surface-mounted PMSM (SPMSM) with equal d-axis and q-axis inductance is studied. The model of PMSM in stationary α-β frame is expressed using complex vectors as follows:

$$\mathbf{u}_s = R_s\mathbf{i}_s + \frac{d\psi_s}{dt} \tag{1}$$

$$\psi_s = L_s i_s + \psi_r \tag{2}$$

where R_s and L_s are the stator resistance and synchronous inductance, respectively; $\mathbf{u}_s$ and $\mathbf{i}_s$ are the stator voltage and current vectors, respectively; ψ_s and ψ_r are the stator and rotor magnet flux linkage vectors, respectively.

By equal-amplitude coordinate transformation, the stator voltage equation of PMSM in synchronous rotating d-q frame can be described as

$$\begin{cases} u_d = R_s i_d + \dfrac{d\psi_{sd}}{dt} - \omega_e\psi_{sq} \\ u_q = R_s i_q + \dfrac{d\psi_{sq}}{dt} + \omega_e\psi_{sd} \end{cases} \tag{3}$$

The stator flux in d-q frame can be described as

$$\begin{cases} \psi_{sd} = L_s i_d + \psi_r \\ \psi_{sq} = L_s i_q \end{cases} \tag{4}$$

From [21], the electromagnetic torque can be expressed as

$$T_e = 1.5p_n\{\psi_r \otimes i_s\} = 1.5p_n\psi_r i_q \tag{5}$$

where u_d and u_q are the dq-axis components of stator voltage, respectively; i_d and i_q are the dq-axis components of stator current, respectively; ψ_{sd} and ψ_{sq} are the dq-axis components of stator flux linkage, respectively; ω_e is the electrical rotor angular velocity; and p_n is the number of pole pairs.

2.2. Flux Prediction Model

Since the mechanical quantities change slowly relative to the electrical quantities, the motor speed can be considered as a constant value within a short time interval. Substituting (4) into (3), eliminating the current variable in the PMSM voltage equation, and performing Euler-forward discretization, the motor flux prediction model can be expressed as follows:

$$\begin{cases} \psi_{sd}(k+1) = T_s u_d(k) + \psi_{sd}(k) + T_s\omega(k)\psi_{sq}(k) - \dfrac{T_s R_s}{L_s}[\psi_{sd}(k) - \psi_r] \\ \psi_{sq}(k+1) = T_s u_q(k) + \psi_{sq}(k) + T_s\omega(k)\psi_{sd}(k) - \dfrac{T_s R_s}{L_s}\psi_{sq}(k) \end{cases} \tag{6}$$

where T_s is the control period.

3. HYBRID-VECTOR MPFC STRATEGY

3.1. VVs Selection and Action Time Calculation

In order to determine VVs quickly and reduce control complexity, a fast selection method for the optimal VV combination based on the sector judgment of the stator flux error vector is proposed in this paper. The details are in the following text.

Eight basic VVs are provided by the three-phase two-level voltage source inverter. Fig. 1 shows the VVs and sector divisions.

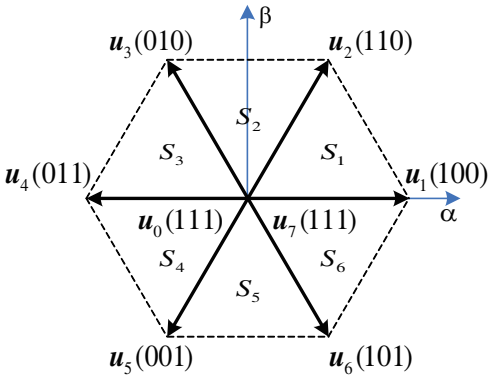

Figure 1. VVs and sector divisions.

The minor voltage drop across the stator resistance can be neglected in the step of vector selection, and the relationship between the stator flux vector and the voltage vector is expressed as

$$\mathbf{u}_s = \frac{d\boldsymbol{\psi}_s}{dt} \tag{7}$$

The Euler-forward discretization of (7) leads to the following equation:

$$\boldsymbol{\psi}_s(k+1) = \boldsymbol{\psi}_s(k) + T_s\mathbf{u}_s(k) \tag{8}$$

Assuming that the rotor of the PMSM rotates counterclockwise, the stator flux vector is in sector S_1, as shown in Fig. 2, where ψ_s^* is the reference of the stator flux vector. According to (8) and Fig. 2, $u_2(110)$ and $u_3(010)$ increase the q-axis stator flux, while $u_5(001)$ and $u_6(101)$ decrease the q-axis stator flux; $u_2(110)$ and $u_6(101)$ increase the d-axis stator flux, while $u_3(010)$ and $u_5(001)$ decrease the d-axis stator flux; $u_0(000)$ and $u_7(111)$ do not change the stator flux vector, but as the rotor rotates, the q-axis stator flux decreases, and the d-axis stator flux increases. So, no matter which sector $\psi_s(k)$ is in and no matter whether the q-axis stator flux ψ_{sq} and the d-axis stator flux ψ_{sd} need to be increased or decreased, there is always a VV that can satisfy the requirement. When a single VV is applied in one control period, only the direction of increase or decrease of ψ_{sq} and ψ_{sd} is correct, but the amount of increase and decrease cannot be precisely controlled. When two VVs are applied in one control period, the direction of ψ_{sq} and ψ_{sd} changes is correct, and the variation of one can be precisely controlled. When three VVs are applied in one control period, two component variations can be precisely controlled simultaneously to achieve deadbeat control of ψ_{sq} and ψ_{sd}, so that torque ripples and current harmonics can be reduced.

As can be seen from Fig. 2, $\Delta\psi_s = \psi_s^* - \psi_s(k)$, $\Delta\psi_s$ is in the second sector at k instant, and the objective is to make ψ_{sq} increase and ψ_{sd} decrease. The active VVs u_2 and u_3 have the same effect on

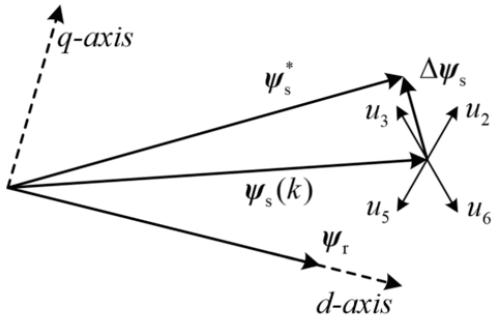

Figure 2. Effect of VV on stator flux vector.

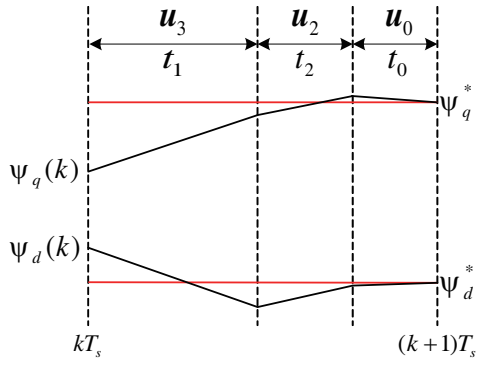

Figure 3. Effect of VV on dq-axis stator flux.

ψ_{sq}, both can increase ψ_{sq}, but have the opposite effects on ψ_{sd}. Therefore, a reasonable allocation of the action time of u_2, u_3, and u_0 can achieve precise control, as shown in Fig. 3.

The relationship between optimal VV combination and sector of stator flux error vector is shown in Table 1.

Table 1. Quick selection.

sector of stator flux error vector	first non-zero VV	second non-zero VV
S_1	$u_1(100)$	$u_2(110)$
S_2	$u_3(010)$	$u_2(110)$
S_3	$u_3(010)$	$u_4(011)$
S_4	$u_5(001)$	$u_4(011)$
S_5	$u_5(001)$	$u_6(101)$
S_6	$u_1(100)$	$u_6(101)$

After the combination of VVs is determined, two adjacent active VVs and one zero VV are applied in one control period to control the stator flux vector. Based on the flux deadbeat principle [30] under the application of three VVs, i.e., $\psi_s^* = \psi_s(k+1)$, the duration of each VV can be calculated, as shown in (9).

$$\begin{cases} d_1\mathbf{M}_1 + d_2\mathbf{M}_2 + d_0\mathbf{M}_0 = \Delta\boldsymbol{\psi}_s \\ d_1 + d_2 + d_0 = 1 \end{cases} \tag{9}$$

where d_1, d_2, and d_0 are the duty cycles of the first active VV, the second active VV, and zero VV, respectively; $\mathbf{M}_1$, $\mathbf{M}_2$, and $\mathbf{M}_0$ are the changes of the flux vector after the first active VV, the second active VV, and zero VV are applied for one control period, respectively; $d_1 = t_1/T_s$, $d_2 = t_2/T_s$, and $d_0 = t_0/T_s$; t_1, t_2, and t_0 are the action time of the first, second, and zero VV, respectively.

3.2. Optimization of Voltage Vectors and Action Time

After obtaining the optimal VVs and action time, the three VVs are sequentially applied to the PMSM using a symmetric pulse width modulation technique in order to further reduce torque ripples and current harmonics. But applying a VV with a short duration may generate narrow pulses. Therefore, the hybrid-vector strategy is proposed to eliminate the application of VVs whose action time is shorter than the set time threshold, correct the selection and action time of the VVs, and prevent the generation of narrow pulses. According to the most restrictive case, the total restriction time affected by dead time compensation and minimum pulse width is $T_{lim} = 2T_{dead} + T_{mpw}$. Here, the time threshold is defined as T_{THR}, whose value depends on T_{lim}. The active VV with a longer action time is defined as u_{opt1} and action time as t_{opt1}, and the shorter one is defined as u_{opt2} and t_{opt2}, respectively. According to the relationship among t_{opt1}, t_{opt2}, t_0, and T_{THR}, the control strategy is divided into the following modes.

1) Strategy when $t_{opt1} > T_{THR}$, $t_{opt2} > T_{THR}$, $t_0 > T_{THR}$.

When the action time of the first VV, the second VV, and zero VV in one control period is longer than T_{THR}, no narrow pulses will be generated at that moment. A three-vector symmetrical modulation strategy is adopted, which is the same as 3VMPC. Taking the stator flux error vector in S_1 as an example, when $u_{opt1} = u_1(100)$ and $t_{opt1} = t_1$, the three-vector symmetric modulation strategy is shown in Fig. 4(a).

The case $t_2 > t_1$ will also occur in S_1, when $u_{opt1} = u_2(110)$, $t_{opt1} = t_2$, and the symmetric modulation strategy is shown in Fig. 4(b). This avoids using only (111) or (000) for zero VV in one sector, balancing the number of switches of the upper and lower switching tubes.

2) Strategy when $t_{opt1} > T_{THR}$, $t_{opt2} < T_{THR}$, $t_0 > T_{THR}$.

When only the action time of the second VV in one period is shorter than T_{THR}, the application of the second VV cannot reach the expected effect and increases the switching frequency of the system. In this case, t_{opt2} is set to 0, and the double-vector modulation strategy with u_{opt1} and zero VV is adopted.

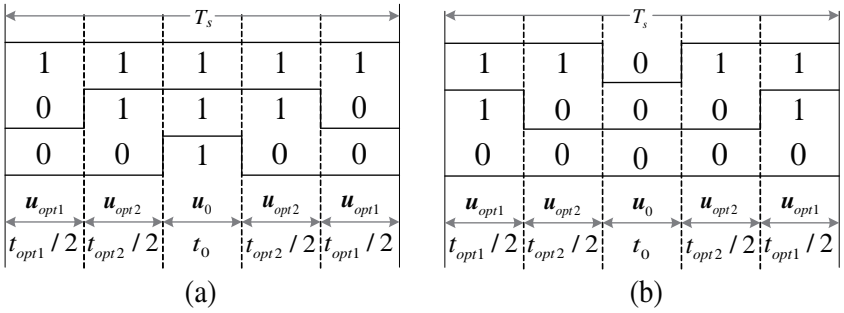

Figure 4. Three-vector modulation strategy. (a) when $u_{opt1} = u_1(100)$, (b) when $u_{opt1} = u_2(110)$.

When applying an active VV and a zero VV in one control period, the direction of ψ_{sq} and ψ_{sd} changes is correct, and the variation of one can be precisely controlled. In order to keep the electromagnetic torque stable in priority, the ψ_{sq} deadbeat principle is adopted to correct the action time, i.e., $\psi_{sq}^* = \psi_{sq}(k+1)$, and the optimization equation is shown in (10).

$$\begin{cases} d_1 M_{1q} + d_0 M_{0q} = \Delta\psi_{sq} \\ d_1 + d_0 = 1 \\ d_2 = 0 \end{cases} \tag{10}$$

Taking S_1 as an example, the modulation strategy is shown in Fig. 5. As can be seen from Fig. 5, the adoption of the double-vector modulation strategy not only suppresses the generation of narrow pulses, but also reduces the switching frequency. Compared with the three-vector modulation strategy, in which two inverter legs change state twice in one control period, the double-vector modulation strategy keeps the state of two inverter legs unchanged, and only one inverter leg changes the state twice in one control period, which reduces the switching frequency by half.

3) Strategy when $t_{opt1} > T_{THR}$, $t_{opt2} > T_{THR}$, $t_0 < T_{THR}$.

When only the action time of zero VV is shorter than T_{THR}, the application of zero VV will generate narrow pulses. Due to the short action time of zero VV, the strategy of only applying two active VVs without zero VV can prevent the generation of narrow pulses and reduce the switching frequency with little impact on the control performance. In this case, t_0 is set to 0, and the double-vector modulation strategy with u_{opt1} and u_{opt2} is adopted, as shown in Fig. 6. In order to keep the torque stable, the action time is optimized using (11).

$$\begin{cases} d_1 M_{1q} + d_2 M_{2q} = \Delta\psi_{sq} \\ d_1 + d_2 = 1 \\ d_0 = 0 \end{cases} \tag{11}$$

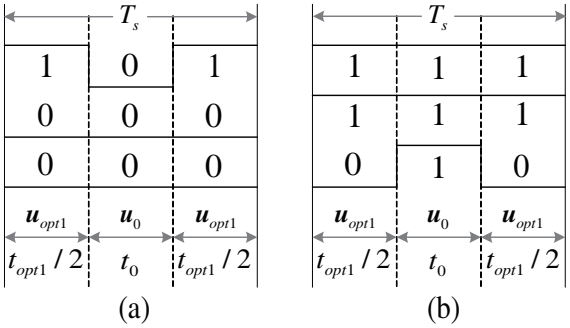

Figure 5. Double-vector modulation strategy. (a) when $u_{opt1} = u_1(100)$, (b) when $u_{opt1} = u_2(110)$.

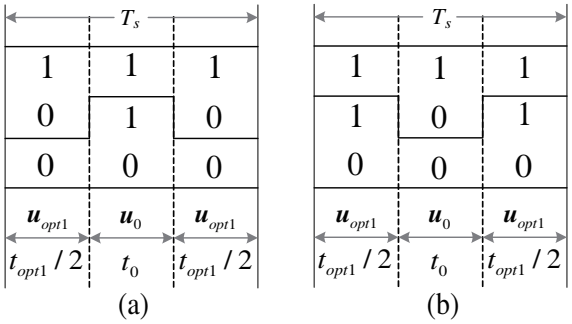

Figure 6. Double-vector modulation strategy. (a) when $u_{opt1} = u_1(100)$, (b) when $u_{opt1} = u_2(110)$.

4) Strategy when $t_{opt1} > T_{THR}$, $t_{opt2} < T_{THR}$, $t_0 < T_{THR}$.

When the action time of both the second optimal VV (the active VV with a shorter action time) and zero VV is shorter than T_{THR}, both the three-vector and two-vector modulation strategies will produce narrow pulses. In this case, a single-vector modulation strategy is adopted, i.e., u_{opt1} is applied to the whole period, eliminating the generation of narrow pulses. Compared with the double-vector modulation strategy, the single-vector modulation strategy does not require switching in one control period and reduces the switching frequency.

5) Strategy when $t_{opt1} < T_{THR}$, $t_{opt2} < T_{THR}$, $t_0 > T_{THR}$.

When the action time of the two active VVs is shorter than T_{THR}, a single-vector modulation strategy is adopted, i.e., the zero VV is applied to the whole period.

In summary, the optimal combination of VVs in each control period switches among single, double, and three VVs, which is determined by the relationship between the action time of three VVs and the set T_{THR}. When the action time of all three VVs is longer than T_{THR}, all three VVs are applied in one control period, as shown in 1). When only one VV action time is shorter than T_{THR}, two VVs are applied in one control period, as shown in 2) and 3). When only one VV action time is longer than T_{THR}, one VV is applied in one control period, as shown in 4) and 5). The proposed hybrid-vector MPFC strategy prevents the generation of narrow pulses and comprehensively considers the VVs distribution and switching states. Hence, the steady-state performance is effectively improved at the same switching frequency compared with 3VMPC. The control diagram of the proposed HV-MPFC strategy is shown in Fig. 7.

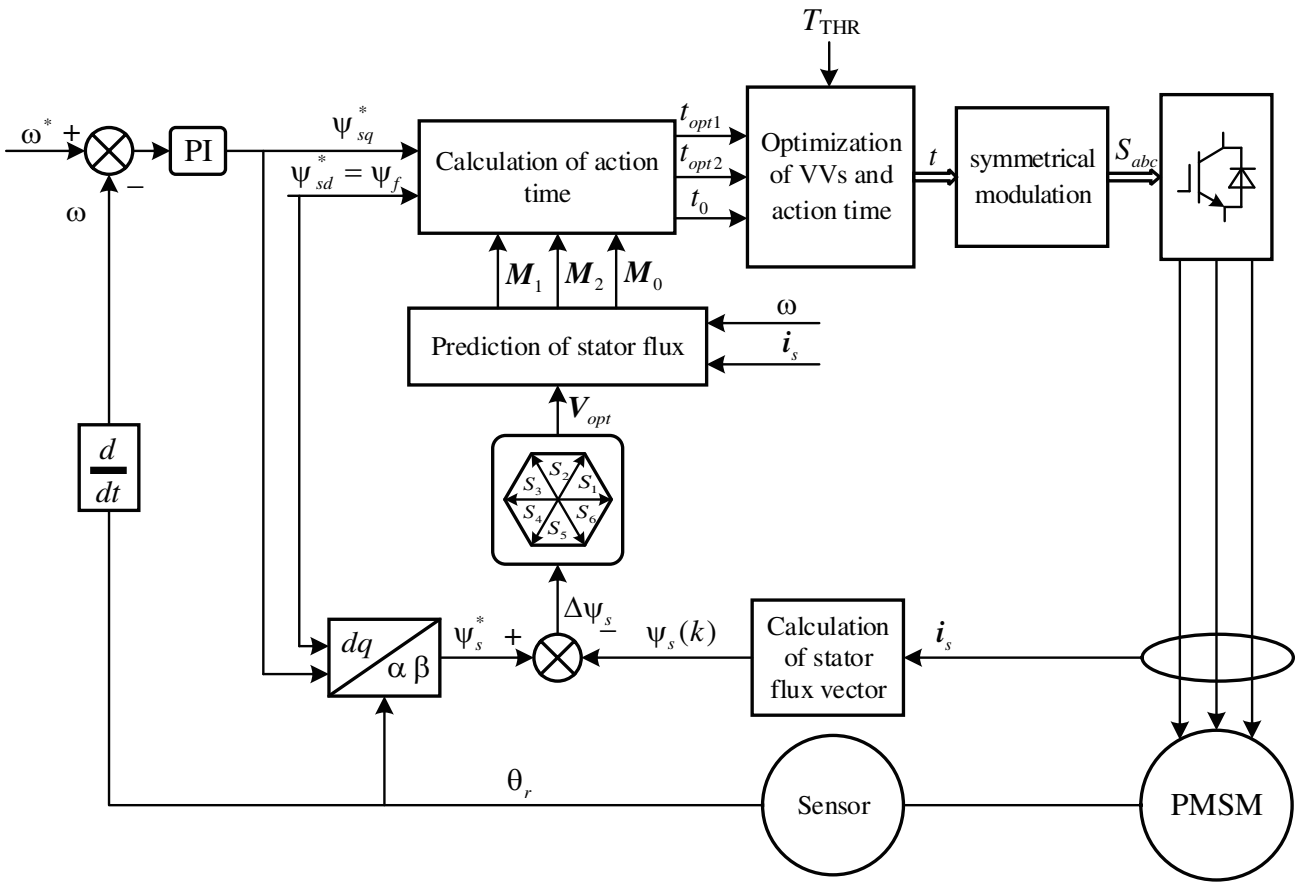

Figure 7. The control diagram of HV-MPFC.

4. EXPERIMENTAL VERIFICATION

To verify the feasibility and effectiveness of the proposed strategy, experiments between 3VMPC and HV-MPFC strategy are carried out based on RT-LAB experimental platform. In the experiments, the IGBT dead time is set to 2.5 µs, and the minimum pulse width is set to 3 µs, and T_{lim} = 8 µs. The experimental platform and surface-mounted PMSM parameters are shown in Fig. 8 and Table 2, respectively.

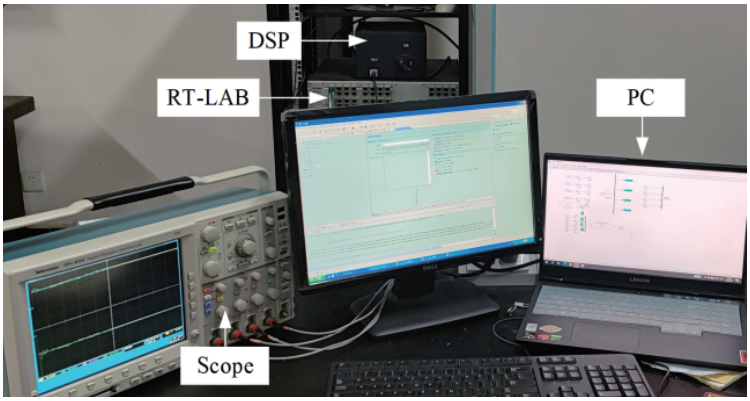

Figure 8. RT-LAB experimental platform.

Table 2. Motor parameters.

Parameter	Description	Value
U_{dc} (V)	DC-bus voltage	310
N (rpm)	Rated Speed	2000
T_L (N·m)	Rated Torque	6
P_n	Number of pole pairs	4
R_s (Ω)	Stator resistance	1.2
L_s (mH)	Synchronous inductance	8.5
ψ_r (Wb)	Permanent magnet flux	0.175
J (kg·m^2)	Moment of Inertia	0.00275

4.1. Performance Comparison between HV-MPFC and 3VMPC

To compare the performance of the two control strategies, steady-state and dynamic experiments are carried out. The time threshold in HV-MPFC is set equal to T_{lim}, i.e., $T_{THR} = T_{lim}$ =8 µs. The steady-state experiments of 3VMPC and HV-MPFC are carried out at the same average switching frequency under two working conditions of 1000 rpm, 4 N·m load and 2000 rpm, 4 N·m load. The steady-state experimental results are shown in Fig. 9 and Fig. 10.

The steady-state experimental results of the drive system running at 1000 rpm and 4 N·m are shown in Fig. 9. In Fig. 9(a), the average switching frequency is 5.42 kHz. It can be observed that there are high harmonics in the stator current when the 3VMPC strategy is adopted, and the Total Harmonic Distortion (THD) of the stator current reaches 6.19%. In the meanwhile, it should be noted that the 3VMPC has large torque ripples and that the tracking inaccuracy of torque reaches 1.01 N·m. In Fig. 9(b), the average switching frequency is 5.41 kHz. When the proposed HV-MPFC method is implemented, it can be seen that the THD of the stator current is decreased to 5.23%, and the torque

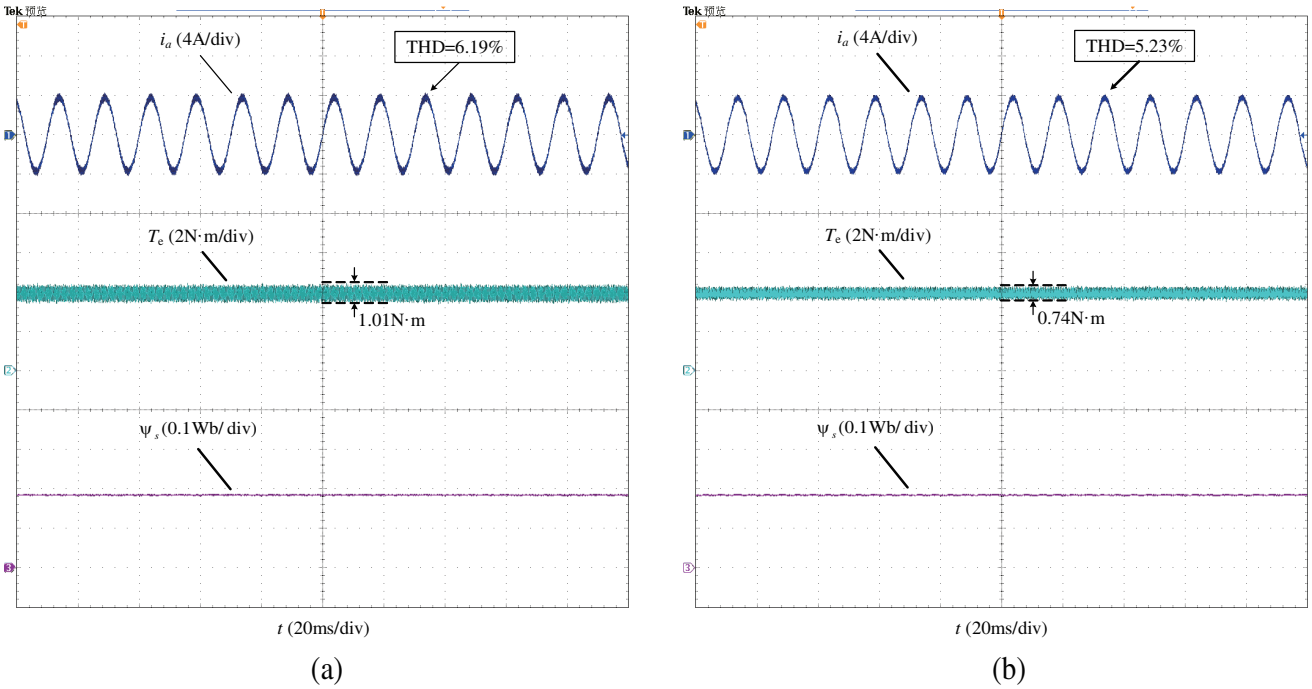

Figure 9. Steady-state experimental results when the drive system operates at 1000 rpm with 4 N·m load. (a) Steady-state experiments of 3VMPC (f_{av} = 5.42 kHz). (b) Steady-state experiments of HV-MPFC (f_{av} = 5.41 kHz).

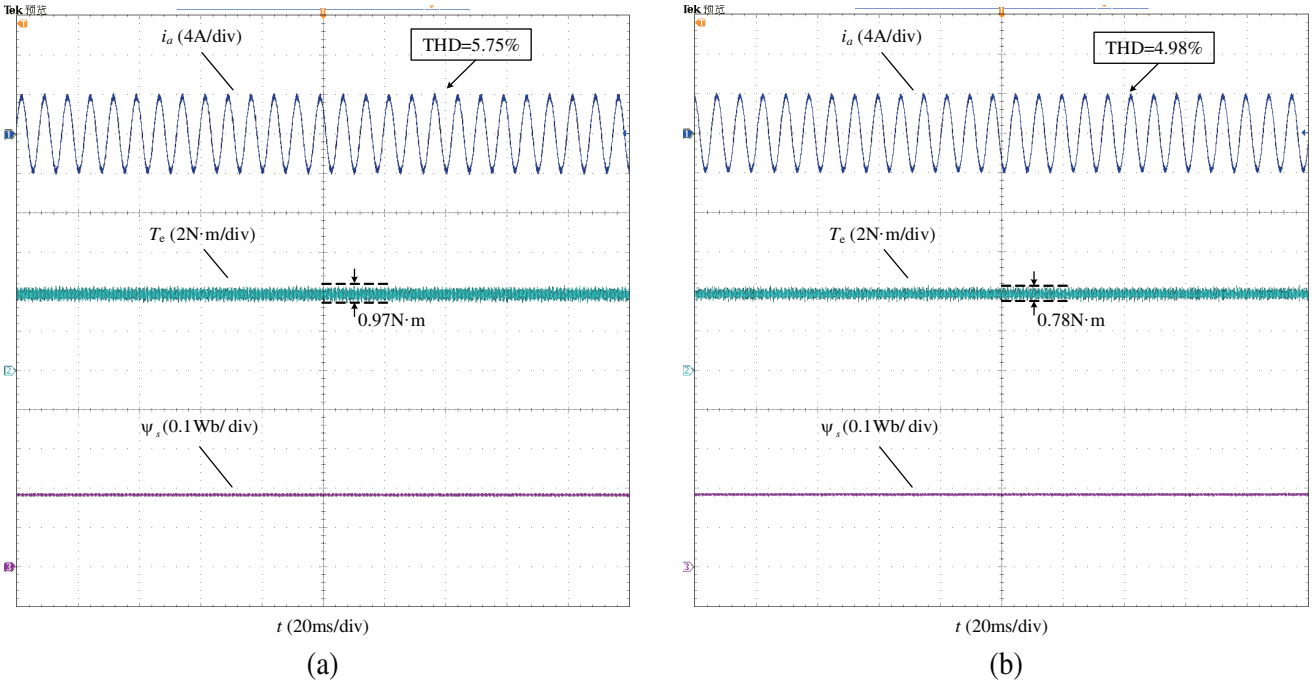

Figure 10. Steady-state experimental results when the drive system operates at 2000 rpm with 4 N·m load. (a) Steady-state experiments of 3VMPC (f_{av} = 5.67 kHz). (b) Steady-state experiments of HV-MPFC (f_{av} = 5.65 kHz).

ripples are reduced to 0.74 N·m. At the same switching frequency, the proposed algorithm reduces the stator current THD and torque ripples, and the control effect is significantly optimized.

The experimental results of the drive system running at 2000 rpm and 4 N·m are shown in Fig. 10, and the average switching frequency is around 5.65 kHz. A similar conclusion can be drawn from the comparison experiments in Figs. 10(a) and 10(b): the proposed HV-MPFC algorithm reduces the stator current THD and the torque ripples and has better steady-state performance than the 3VMPC strategy at the same switching frequency. Table 3 visually demonstrates the superiority of the proposed HV-MPFC strategy in this paper.

Table 3. Steady-state experimental results of 3VMPC and HV-MPFC.

Number	f_{av}/kHz	ΔT_e/N·m	Optimization/%	THD/%	Optimization/%
9(a)	5.42	1.01	-	6.19	-
9(b)	5.41	0.74	26.73	5.23	15.51
10(a)	5.67	0.97	-	5.75	-
10(b)	5.65	0.78	19.6	4.98	13.39

After comparing the steady-state performances of the two control strategies, a comparison of the dynamic performance is necessary. Fig. 11 shows the dynamic performance comparison results of the two control strategies when motor speed is 1000 rpm, and motor load is stepped from 0 to 4 N·m and 2 N·m in sequence. From Figs. 11(a) and (b), it can be observed that after the torque reference step from 0 to 4 N·m, both strategies can quickly track their reference values in about 0.43 ms. Therefore, the HV-MPFC strategy can obtain similar dynamic performance to the 3VMPC strategy.

Next, the speed test is carried out to further verify the performance of the proposed strategy. In Fig. 12, the speed reference suddenly changes from 1000 rpm to 1500 rpm with a load of 4 N·m. It can be

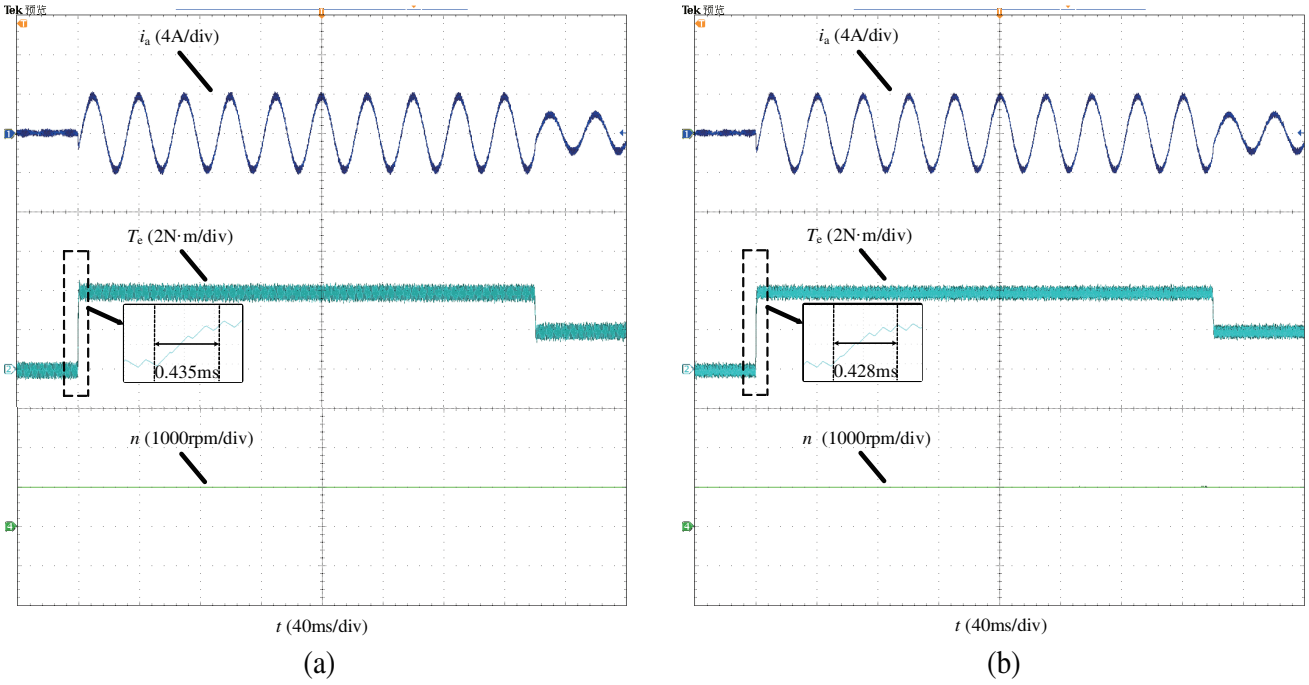

Figure 11. Dynamic experimental results when the load torque is stepped from 0 to 4 N·m and 2 N·m in sequence. (a) Dynamic experiments of 3VMPC (f_{av} = 5.42 kHz). (b) Dynamic experiments of HV-MPFC (f_{av} = 5.41 kHz).

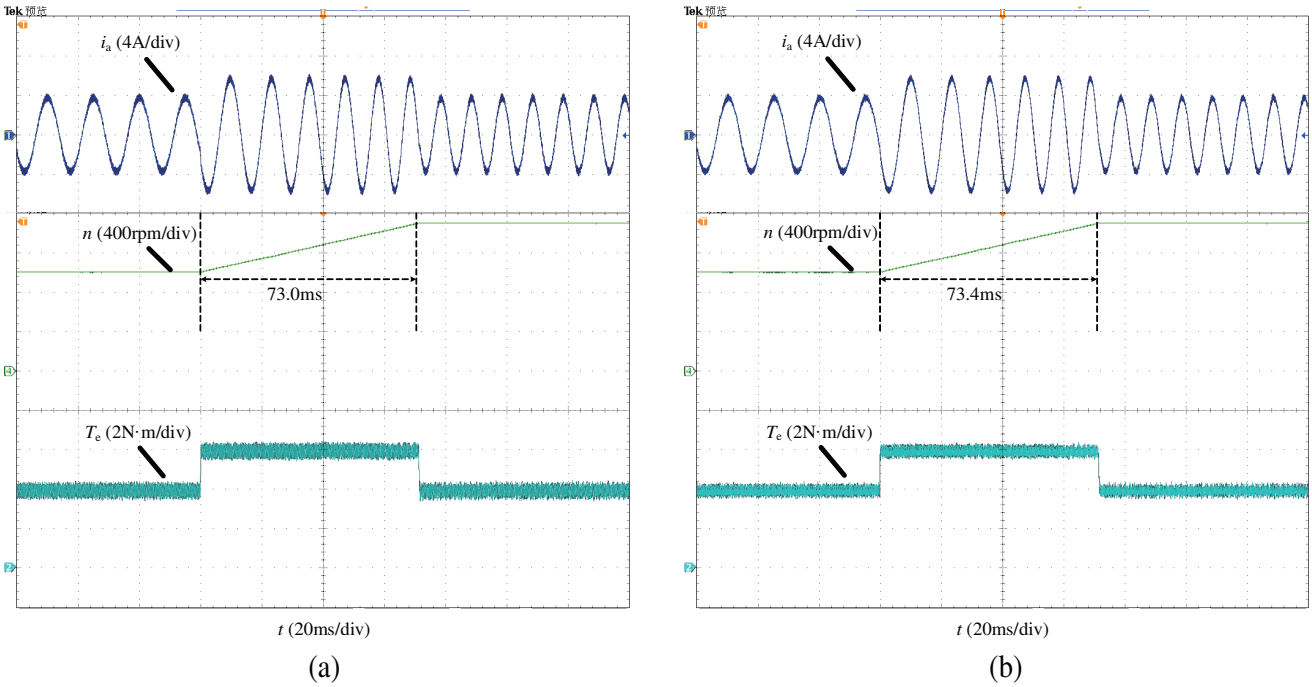

Figure 12. Dynamic experimental results when the speed changes from 1000 rpm to 1500 rpm. (a) Dynamic experiments of 3VMPC (f_{av} = 5.42 kHz). (b) Dynamic experiments of HV-MPFC (f_{av} = 5.41 kHz).

observed that both control strategies can drive the PMSM to make the speed track the reference value promptly about 73 ms, and the HV-MPFC method proposed in this paper has a more stable torque control performance than 3VMPC. Thus, the proposed HV-MPFC strategy achieves good steady-state and dynamic control and effectively improves the control accuracy.

4.2. Controller Performance at Different T_{THR}

In order to compare the controller performance of the proposed algorithm at different T_{THR}, 4 sets of comparison experiments were carried out at different time thresholds. T_{THR} is set to 0 µs, 8 µs, 15 µs, and 20 µs, respectively, and the control frequency is set to 10 kHz (the HV-MPFC of 0 µs corresponds to the 3VMPC). The motor speed and load are 1000 rpm and 4 N·m, respectively. Fig. 13 shows the experimental waveforms of motor stator current, electromagnetic torque and switching frequency in 4 cases, respectively.

As can be seen from Fig. 13, with the increase of T_{THR}, the switching frequency decreases greatly; the stator current harmonics increase slowly; and the torque ripples are basically unchanged within 0.8 N·m at $T_{THR} \leq 15$ µs. Large torque ripples that can occasionally approach 1.58 N·m are present when $T_{THR} = 20$ µs. The large torque ripples arise due to an increase in T_{THR}, which makes the system more likely to adopt single-vector strategy to lower switching frequency.

In the inverter control system, the two indicators, stator current harmonics and torque ripples, are in contradiction with the switching frequency indicator. In order to compare the steady-state performance of controllers corresponding to different T_{THR}, it is necessary to define an evaluation function to quantify the performance of the control system. The focus on current harmonics, torque ripples, and switching frequency varies in different application situations and should be adjusted flexibly. In this paper, the evaluation function is designed with reference to the per-unit value; the torque base value is rated torque 6 N·m; and the switching frequency base value is 6.67 kHz. The evaluation function is as follows:

$$E = \frac{\Delta T_e}{6} + \frac{f_{av}}{6.67} + \frac{THD}{100} \tag{12}$$

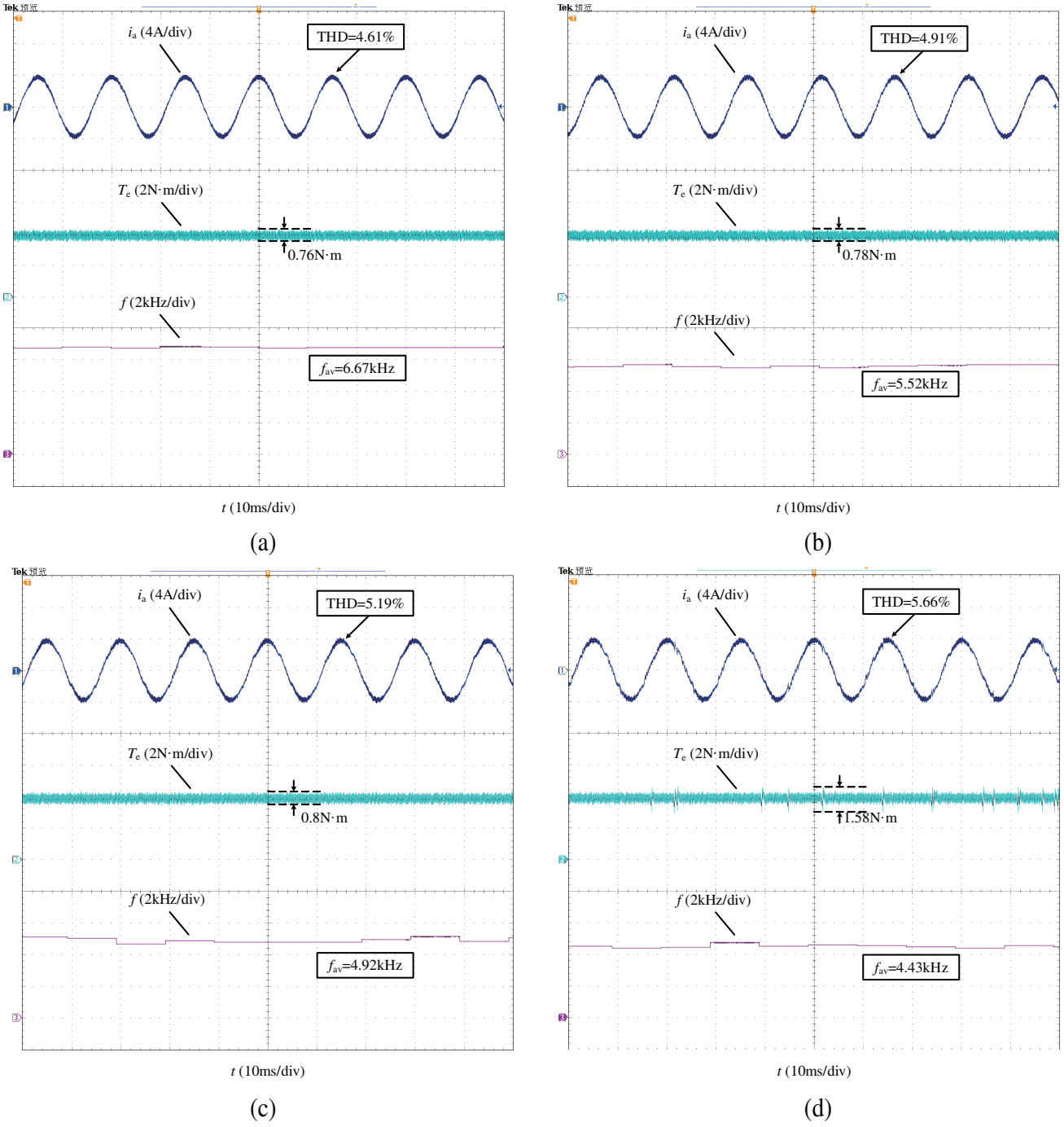

Figure 13. Experimental waveforms of current, torque and switching frequency of HV-MPFC with different T_{THR}. (a) Experimental results of HV-MPFC (T_s =100 μs, T_{THR} =0 μs). (b) Experimental results of HV-MPFC (T_s =100 μs, T_{THR} =8 μs). (c) Experimental results of HV-MPFC (T_s = 100 μs, T_{THR} = 15 μs). (d) Experimental results of HV-MPFC (T_s = 100 μs, T_{THR} = 20 μs).

As can be seen from (12), the lower value of the function indicates better steady-state performance. The values of the evaluation function corresponding to the 4 different T_{THR} are shown in Table 4. From Table 4, it can be seen that under this evaluation system, the evaluation function value reaches the minimum value when T_{THR} =15 μs. Therefore, the introduction of T_{THR} not only prevents

Table 4. Steady-state performance of different T_{THR}.

T_{THR}/μs	ΔT_e/N·m	f_{av}/kHz	THD of current/%	E
	0.76	6.67	4.61	1.17
8	0.78	5.52	4.91	1.01
15	0.80	4.92	5.19	0.92
20	1.58	4.43	5.66	0.98

the generation of narrow pulses, but also enables flexible adjustment of the contradiction of current harmonics and torque ripples vs switching frequency, making it possible to reduce the system switching frequency without significantly increasing the stator current harmonics and torque ripples, which is an advantage that the 3VMPC does not have.

5. CONCLUSION

For reducing the computational burden and preventing the generation of narrow pulses, a hybrid-vector model predictive flux control strategy is proposed in this paper. The main contributions of this achievement include the following:

1) HV-MPFC can quickly select the optimal voltage vector by judging the sector where the stator flux error vector is located with only one prediction calculation, reducing the computational burden compared to 3VMPC.

2) By eliminating the VVs whose action time is shorter than the set time threshold, a hybrid-vector strategy to switch among three VVs, two VVs, and a single VV is adopted. The HV-MPFC strategy suppresses the generation of narrow pulses and achieves smaller torque ripples and stator current harmonics at the same switching frequency than 3VMPC.

3) By selecting an appropriate T_{THR}, the HV-MPFC strategy can greatly reduce the switching frequency while maintaining small current harmonics and electromagnetic torque ripples.

ACKNOWLEDGMENT

This work was supported by the Natural Science Foundation of Hunan Province of China under Grant Number 2022JJ50094.

REFERENCES

1. Bi, G., Q. Wang, D. Ding, et al., "Multi-optimization objective online tracking-based parameter self-tuning method for sensorless PMSM drives," *IEEE Transactions on Transportation Electrification*, Vol. 9, No. 1, 1390–1402, Mar. 2023.
2. Zhang, R., Z. Yin, N. Du, J. Liu, and X. Tong, "Robust adaptive current control of a 1.2-MW direct-drive PMSM for traction drives based on internal model control with disturbance observer," *IEEE Transactions on Transportation Electrification*, Vol. 7, No. 3, 1466–1481, Sept. 2021.
3. Murshid, S., and B. Singh, "Implementation of PMSM drive for a solar water pumping system," *IEEE Transactions on Industry Applications*, Vol. 55, No. 5, 4956–4964, Sept.–Oct. 2019.
4. Wang, G., M. Valla, and J. Solsona, "Position sensorless permanent magnet synchronous machine drives — A review," *IEEE Transactions on Industrial Electronics*, Vol. 67, No. 7, 5830–5842, Jul. 2020.
5. Wang, W., H. Yan, Y. Xu, et al., "New three-phase current reconstruction for pmsm drive with hybrid space vector pulsewidth modulation technique," *IEEE Transactions on Power Electronics*, Vol. 36, No. 1, 662–673, Jan. 2021.

6. Casadei, D., F. Profumo, G. Serra, and A. Tani, "FOC and DTC: two viable schemes for induction motors torque control," *IEEE Transactions on Power Electronics*, Vol. 17, No. 5, 779–787, Sept. 2002.
7. Zhang, X. and Y. He, "Direct voltage-selection based model predictive direct speed control for PMSM drives without weighting factor," *IEEE Transactions on Power Electronics*, Vol. 34, No. 8, 7838–7851, Aug. 2019.
8. Yu, F., S. Zhao, Z. Tian, and X. Wu, "Model predictive flux control of semicontrolled open-winding PMSG with circulating current elimination," *IEEE Transactions on Industrial Informatics*, Vol. 17, No. 2, 1438–1448, Feb. 2021.
9. Ge, L., J. Zhong, J. Huang, N. Jiao, S. Song, and R. W. De Doncker, "A novel model predictive torque control of SRMs with low measurement effort," *IEEE Transactions on Industrial Electronics*, Vol. 70, No. 4, 3561–3570, Apr. 2023.
10. Zhang, Y., D. Xu, and L. Huang, "Generalized multiple-vector-based model predictive control for PMSM drives," *IEEE Transactions on Industrial Electronics*, Vol. 65, No. 12, 9356–9366, Dec. 2018.
11. Zhang, X. and B. Hou, "Double vectors model predictive torque control without weighting factor based on voltage tracking error," *IEEE Transactions on Power Electronics*, Vol. 33, No. 3, 2368–2380, Mar. 2018.
12. Osman, I., D. Xiao, K. S. Alam, S. M. S. I. Shakib, M. P. Akter, and M. F. Rahman, "Discrete space vector modulation-based model predictive torque control with no suboptimization," *IEEE Transactions on Industrial Electronics*, Vol. 67, No. 10, 8164–8174, Oct. 2020.
13. Zhang, X. and Z. Zhao, "Multi-stage series model predictive control for PMSM drives," *IEEE Transactions on Vehicular Technology*, Vol. 70, No. 7, 6591–6600, Jul. 2021.
14. Sun, X., T. Li, M. Yao, G. Lei, Y. Guo, and J. Zhu, "Improved finite-control-set model predictive control with virtual vectors for PMSHM drives," *IEEE Transactions on Energy Conversion*, Vol. 37, No. 3, 1885–1894, Sept. 2022.
15. Zhang, Y., D. Xu, J. Liu, S. Gao, and W. Xu, "Performance improvement of model-predictive current control of permanent magnet synchronous motor drives," *IEEE Transactions on Industry Applications*, Vol. 53, No. 4, 3683–3695, Jul.–Aug. 2017.
16. Zhao, W., H. Wang, T. Tao, and D. Xu, "Model Predictive torque control of five-phase PMSM by using double virtual voltage vectors based on geometric principle," *IEEE Transactions on Transportation Electrification*, Vol. 7, No. 4, 2635–2644, Dec. 2021.
17. Kang, S.-W., J.-H. Soh, and R.-Y. Kim, "Symmetrical three-vector-based model predictive control with deadbeat solution for IPMSM in rotating reference frame," *IEEE Transactions on Industrial Electronics*, Vol. 67, No. 1, 159–168, Jan. 2020.
18. Wang, C., J. Ji, H. Tang, T. Tao, and W. Zhao, "Improved model predictive current control for linear vernier permanent-magnet motor with efficient voltage vectors selection," *IEEE Transactions on Industrial Electronics*, Vol. 70, No. 3, 2833–2842, Mar. 2023.
19. Yu, F., K. Li, Z. Zhu, and X. Liu, "An over-modulated model predictive current control for permanent magnet synchronous motors," *IEEE Access*, Vol. 10, 40391–40401, 2022.
20. Gu, M., Y. Yang, M. Fan, et al., "Finite control set model predictive torque control with reduced computation burden for PMSM based on discrete space vector modulation," *IEEE Transactions on Energy Conversion*, Vol. 38, No. 1, 703–712, Mar. 2023.
21. Jin, T., H. Song, D. L. Mon-Nzongo, P. G. Ipoum-Ngome, H. Liao, and M. Zhu, "Virtual three-level model predictive flux control with reduced computational burden and switching frequency for induction motors," *IEEE Transactions on Power Electronics*, Vol. 38, No. 2, 1571–1582, Feb. 2023.
22. Li, X., Z. Xue, L. Zhang, and W. Hua, "A low-complexity three-vector-based model predictive torque control for SPMSM," *IEEE Transactions on Power Electronics*, Vol. 36, No. 11, 13002–13012, Nov. 2021.
23. Xu, B., Q. Jiang, W. Ji, and S. Ding, "An improved three-vector-based model predictive current control method for surface-mounted PMSM drives," *IEEE Transactions on Transportation Electrification*, Vol. 8, No. 4, 4418–4430, Dec. 2022.

24. Petkar, S. G. and V. K. Thippiripati, "Effective multivector-operated predictive current control of PMSM drive with reduced torque and flux ripple," *IEEE Transactions on Transportation Electrification*, Vol. 9, No. 2, 2217–2227, Jun. 2023.
25. Amiri, M., J. Milimonfared, and D. A. Khaburi, "Predictive torque control implementation for induction motors based on discrete space vector modulation," *IEEE Transactions on Industrial Electronics*, Vol. 65, No. 9, 6881–6889, Sept. 2018.
26. Wang, Y., X. Wang, W. Xie, et al., "Deadbeat model-predictive torque control with discrete space-vector modulation for PMSM drives," *IEEE Transactions on Industrial Electronics*, Vol. 64, No. 5, 3537–3547, May 2017.
27. Yang, Y., H. Wen, M. Fan, M. Xie, and R. Chen, "Fast finite-switching-state model predictive control method without weighting factors for T-type three-level three-phase inverters," *IEEE Transactions on Industrial Informatics*, Vol. 15, No. 3, 1298–1310, Mar. 2019.
28. Park, D.-M. and K.-H. Kim, "Parameter-independent online compensation scheme for dead time and inverter nonlinearity in IPMSM drive through waveform analysis," *IEEE Transactions on Industrial Electronics*, Vol. 61, No. 2, 701–707, Feb. 2014.
29. Leggate, D. and R. J. Kerkman, "Pulse-based dead-time compensator for PWM voltage inverters," *IEEE Transactions on Industrial Electronics*, Vol. 44, No. 2, 191–197, Apr. 1997.
30. Li, X., Z. Xue, X. Yan, et al., "Voltage vector rapid screening-based three-vector model predictive torque control for permanent magnet synchronous motor," *Transactions of China Electrotechnical Society*, Vol. 37, No. 7, 1666–1678, 2022.